as it penetrates into the lower mantle.

Our results suggest another mechanism of softening that is independent of grain size: softening due to a structural phase transformation (from the orthorhombic to the tetragonal structure). The phase transformations in perovskites are in general close to second order and involve only a small rearrangements of atoms. Thus, in contrast to the (first-order) transformation from spinel to perovskite + magnesiowustite, no grain-size reduction is found associated with the structural phase transformation from the orthorhombic to tetragonal structure. Therefore, the enhancement of creep due to this structural phase transformation must be due to the enhancement of diffusion.

Diffusion creep in fine-grained aggregates has been observed in many solids, and it is not surprising to see a similar behavior in perovskite. A real question, however, is how close are the transition conditions between diffusion and dislocation creep for perovskite to the conditions in Earth. Our results show that diffusion creep dominates in perovskite over a wide range of conditions and a linear, grain size–dependent rheology is likely to be an important deformation mechanism in a large part of the lower mantle.

Our results suggest two mechanisms of rheological softening: one due to grain-size reduction and the other due to a structural phase transformation. Both are likely to occur in the shallow portions of the lower mantle (*4, 7*). Therefore, rheologically soft layers may occur in the top portions of the lower mantle, which would act to decouple the convective motion between the upper and lower mantle (*19*).

The use of analog material to infer the lower mantle rheology has large uncertainties. We suggest that the presence or absence of seismic anisotropy in the lower mantle should provide an important clue on the dominant mechanisms of deformation: little preferred orientation of perovskite would occur and hence little seismic anisotropy would be observed if the deformation mechanism is diffusion creep, whereas dislocation creep would result in a significant preferred orientation and the resultant seismic anisotropy (*20*).

REFERENCES AND NOTES

1. U. R. Christensen and D. A. Yuen, *J. Geophys. Res.* **94**, 814 (1989); A. P. van den Berg, D. A. Yuen, P. E. van Keken, *Geophys. Res. Lett.* **18**, 2197 (1992).
2. S. M. Schmid, J. N. Boland, M. S. Paterson, *Tectonophysics* **43**, 257 (1977); S. Karato, M. S. Paterson, J. D. Fitz Gerald, *J. Geophys. Res.* **91**, 8151 (1986); J. Tullis and R. A. Yund, *J. Struct. Geol.* **13**, 987 (1991).
3. D. C. Rubie, *Nature* **308**, 505 (1984).
4. E. Ito and H. Sato, *ibid.* **351**, 140 (1991).
5. N. Doukhan and J. C. Doukhan, *Phys. Chem. Minerals* **13**, 403 (1986); J. P. Poirier, S. Beauchesne, F. Guyot, in *Perovskite: A Structure of Great Importance to Geophysics and Materials Science*, A. Navrotsky and D. J. Weidner, Eds. (American Geophysical Union, Washington, DC, 1989), pp. 119–123.
6. E. Ito and Y. Matsui, *Earth Planet. Sci. Lett.* **38**, 443 (1978); T. Yagi, H.-K. Mao, P. M. Bell, *Phys. Chem. Minerals* **3**, 97 (1978).
7. G. H. Wolf and M. S. T. Bukowinski, in *High Pressure Research in Mineral Physics*, Y. Syono and M. H. Manghnani, Eds. (American Geophysical Union, Washington, DC, 1987), pp. 313–331; Y. Wang, F. Guyot, A. Yeganeh-Haeri, R. C. Liebermann, *Science* **248**, 468 (1990); X. Liu and R. C. Liebermann, *Eos* **69**, 1451 (1988).
8. S. Karato, K. Fujino, E. Ito, *Geophys. Res. Lett.* **17**, 13 (1990).
9. U. Balachandran, B. Odekirk, N. G. Eror, *J. Solid State Chem.* **41**, 185 (1982); G. V. Lewis and C. R. A. Catlow, *J. Phys. Chem. Solids* **47**, 89 (1986); A. Wall and G. D. Price, *Phys. Earth Planet. Inter.* **58**, 192 (1989).
10. Pores occur both inside the grains and at grain boundaries. Deformation experiments were carried out at up to 30% strain without fracture. Also, the results on specimens with different porosities are indistinguishable. Thus we believe that the mechanical data are largely free from the effects of porosity.
11. H. J. Frost and M. F. Ashby, *Deformation Mechanism Maps* (Pergamon, Oxford, 1982), chaps. 2 and 18.
12. Grain growth from ~11 to ~13 μm occurred during the course of the deformation experiment, which accounts for an ~40% change in creep rate. The grain size shown in Fig. 3 is the starting grain size.
13. Both the $\{110\}\langle 1\bar{1}0\rangle$ and $\{100\}\langle 001\rangle$ slip systems operate in perovskites [the slip systems are referred to the corresponding cubic lattice (*5*)]. At high temperatures, the $\{110\}\langle 1\bar{1}0\rangle$ slip system is stronger than the $\{100\}\langle 001\rangle$ slip system [*5*; K. Wright, thesis, University of London (1991)]. Therefore, the $\{110\}\langle 1\bar{1}0\rangle$ slip system is assumed to control the creep strength of a polycrystal (*11*). Wright observed no significant effect of phase transformations on dislocation creep, and her dislocation creep data apply to both orthorhombic and tetragonal phases.
14. Frost and Ashby (*11*) and S. Karato [*Phys. Earth Planet. Inter.* **55**, 234 (1989)] discussed the systematics of creep properties. A. M. Brown and M. F. Ashby [*Acta Metall.* **28**, 1085 (1980)] examined the correlation in diffusion coefficients with crystal structure and bonding. These studies suggest that creep properties of materials with the same crystal structure and chemical bonding will be similar at the same homologous temperatures (T/T_m).
15. R. Jeanloz and S. Morris, *Annu. Rev. Earth Planet. Sci.* **14**, 377 (1986); E. Ito and T. Katsura, *Geophys. Res. Lett.* **16**, 425 (1989).
16. The stress magnitude σ in the mantle may be estimated from the viscosity η and the strain rate $\dot{\varepsilon}$ from $\sigma \sim \dot{\varepsilon}$. Choosing $\eta = 10^{21}$ to 10^{22} Pa·s [W. R. Peltier, in *Mantle Convection*, W. R. Peltier, Ed. (Gordon and Breach, New York, 1989), pp. 389–478] and $\dot{\varepsilon} = 10^{-15}$ s^{-1} (estimated from the velocity of plates and the depth of the mantle), one gets $\sigma = 1$ to 10 MPa (or $\sigma/\mu = 10^{-4}$ to 10^{-5}).
17. H. G. Ave' Lallemant, J. C. Mercier, N. L. Carter, J. V. Ross, *Tectonophysics* **70**, 85 (1980); S. Karato, *ibid.* **104**, 155 (1984).
18. I-W. Chen and L. A. Xue, *J. Am. Ceram. Soc.* **73**, 2585 (1990).
19. The presence of a low-viscosity layer at the top of the lower mantle or at the base of the upper mantle is suggested by the theoretical analysis of geoid by A. M. Forte, A. M. Dziewonski, and R. L. Woodward [in *Proceedings of IUGG Symposium 6*, J.-L. Le Mouel, Ed. (International Union of Geodesy and Geophysics, Brussels, in press)].
20. S. Karato, *Phys. Earth Planet. Inter.* **51**, 107 (1988).

21. We thank K. Wright for providing unpublished data on creep in single-crystal $CaTiO_3$, D. L. Kohlstedt for the use of some of his experimental facilities and for reading the earlier version of the manuscript, D. A. Yuen, A. M. Forte, and Y. Wang for stimulating discussions, and Q. Bai and Z. Wang for assistance in the laboratory studies. J. Tullis's constructive criticism was particularly helpful in improving the paper. This research is supported by the National Science Foundation through grant EAR-9005279.

8 October 1991; accepted 3 January 1992

Mechanics of Wind Ripple Stratigraphy

SPENCER B. FORREST AND PETER K. HAFF*

Stratigraphic patterns preserved under translating surface undulations or ripples in a depositional eolian environment are computed on a grain by grain basis using physically based cellular automata models. The spontaneous appearance, growth, and motion of the simulated ripples correspond in many respects to the behavior of natural ripples. The simulations show that climbing strata can be produced by impact alone; direct action of fluid shear is unnecessary. The model provides a means for evaluating the connection between mechanical processes occurring in the paleoenvironment during deposition and the resulting stratigraphy preserved in the geologic column: vertical compression of small laminae above a planar surface indicates nascent ripple growth; supercritical laminae are associated with unusually intense deposition episodes; and a plane erosion surface separating sets of well-developed laminae is consistent with continued migration of mature ripples during a hiatus in deposition.

LOOSE GRANULAR BEDS OFTEN RESPOND to the presence of a moving fluid by assuming characteristic regular undulations called ripples, megaripples, sandwaves, antidunes, or dunes, depending on their size and genesis (*1, 2*). In a depositional environment, slight variations with time in the mean grading, orientation, packing, or mineral content of the surficial grains may be preserved in the accumulating column of sediment as the individual laminae; collectively these make up the strata observed in clastic sedimentary rocks. Knowledge of the fluid and sediment conditions that can lead to stratigraphic patterns in rocks would make it possible to assess the paleomechanical conditions under which the

Department of Civil and Environmental Engineering, Duke University, Durham, NC 27706.

*To whom correspondence should be addressed.

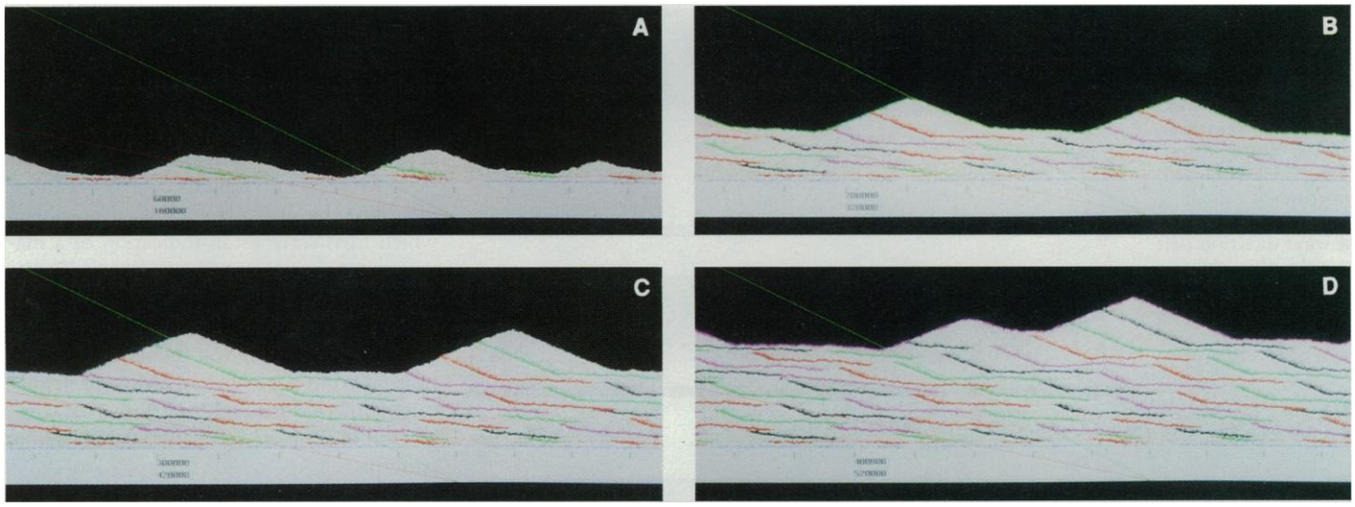

Fig. 1. Simulation showing the configuration of subcritically climbing ripples after increments of (**A**) 100, (**B**) 130, (**C**) 160, and (**D**) 180 saltation impacts per surface grain site; a (late) ripple merger is captured in (D). Surface grains are periodically stained different colors to indicate instantaneous depositional surfaces. Long straight faint lines show angle of repose (34°) and impact angle (11.5°). Wind direction and ripple motion are left to right.

constituent rock was originally laid down and, in turn, the paleoenvironment.

Wind ripples (*3*) form when a sufficiently strong wind blows across a dry sandy surface. Mature ripples are typically 7 to 14 cm in wavelength and 0.5 to 1.0 cm in amplitude. Ripples form when wind-blown, high-speed saltating grains obliquely strike a sandy bed and impel other grains forward. On an initially flat surface, individual impacts generate small depressions and zones of uneven small-scale topography. Surface areas sloping upwind then tend to be impacted more frequently than horizontal or downwind-oriented surfaces. The saltating grain typically rebounds a great distance downwind, whereas low-energy reptating grains are impelled forward a few to as many as a few hundred grain diameters d (d = 0.02 to 0.04 cm for a fine sand). Some of the reptating grains originating on an upwind slope come to rest on an adjacent downwind slope, where their probability of reentrainment is lower than that of upwind grains freshly exposed. Consequently, the nascent ripples begin to grow in size and to move in the downwind direction. This behavior is dominated by grain impact and not by direct fluid stress.

The model simulations follow the time history of each individual grain that ultimately makes up a small sample of the sedimentary deposit. The ejection into the airstream of sand grains from a loose, sandy surface by the impact of a high-speed, windblown sand grain is quantified by the splash function (*4*), the number of grains ejected in a particular velocity range as a function of impact velocity. The splash function, which encapsulates much of the mechanical response of a sand bed to a sand-moving wind, has been studied experimentally (*5, 6*) and through simulations (*7, 8*). From direct simulations of the impact process (*7*) we estimated that the mean number of ejected grains per impact for sand of diameter 0.23 mm would increase approximately linearly from about 3 (0 to 7) grains at an impact speed of 2 m s^{-1} to about 10 (0 to 22) grains at 6 m s^{-1} (variation in mean values is shown in parentheses). The number of ejecta increases slightly for a sand of diameter 0.32 mm. Typical calculated ejection speeds for these impact conditions ranged from 0.3 to about 0.4 m s^{-1}. Ejection angles typically exceeded 50°, measured from the downstream horizontal, for all impact velocities, but with large fluctuations. In our simulations, the properties of ejected particles were selected stochastically from the appropriate splash rule distribution for each impact. In order to limit the size of the simulation, impacting particles were given identical velocities (3 m s^{-1}) and impact angles (11.5°).

With this approach (*9*), the basic kinds of stratification produced by the advance of wind ripples (*10*) can be reproduced. At the same time, the detailed dynamics of the particles over the period during which the sedimentary features are being constructed is recoverable. This means that a discrepancy in form between a set of simulated strata and the corresponding natural strata may ultimately be traced to errors in assumptions about the environmental conditions under which the natural strata were produced and upon which simulations are based. We focused on wind ripples because much of their mechanics is understood. Similar models could be applied to subaqueous ripple stratigraphy, except that direct fluid stress would dominate impact as a transport mechanism.

We first examined the development of ripples on an initially flat bed responding to a sand-laden wind (Fig. 1, A through D). In the simulations, a mottled surface gradually evolved by the merger of small bed undulations into a regular ripple train. Ripples grow because of the geometrical effect of greater impact and ejection flux on upwind-oriented slopes than on downwind-oriented slopes. Mergers occurred when two adjacent ripples "collided" and became one. This happened frequently for small nascent ripples because of random fluctuations in the impact rate and because ripples of uneven size move at different mean forward speeds; smaller bedforms translated faster because they contain less material to be processed by impacts. Large ripples, on the other hand, are not so susceptible to fluctuations in the impact rate and are further stabilized by the saltation dynamics: if one ripple begins to gradually overtake a slightly larger one, the incorporation of material from the leeward ripple into the windward one effectively exchanges their relative sizes, and thus their relative speeds. Hence, impact dynamics tend automatically to filter out ripples of significantly disparate sizes (by merger) and to stabilize a field of nearly equally spaced and equally sized mature bedforms at a constant number of ripples per unit length. These two factors combine to produce the striking ripple patterns commonly observed on dry sand.

During a single simulation we periodically "stained" the uppermost grain layer of the instantaneous surface of the ripple train with

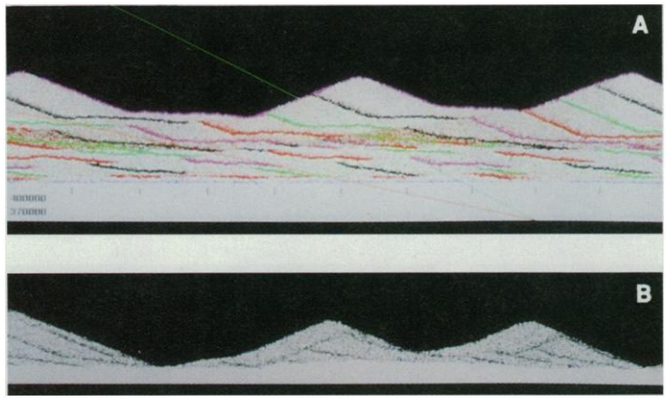

Fig. 2. Simulations of ripple response to a variable deposition rate. (**A**) A hiatus in deposition (but not wind speed) shows up as an erosion surface truncating well-developed, subcritically climbing laminae; (**B**) reversal of wind direction (left to right, then right to left) on an otherwise subcritically climbing ripple.

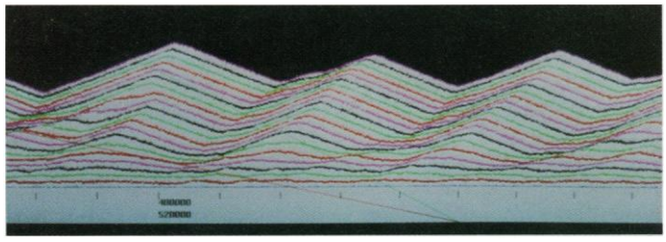

Fig. 3. Simulations showing the result of a high rate of deposition of blowing sand on slowly translating ripples (supercritical climbing).

a distinctive color in order to allow some tracking of grain positions (Fig. 1). As a stained surface eroded on the stoss (upwind) side, the eroded grains migrated over the ripple crest, where they became lodged relatively undisturbed in the impact shadow on the lee slope.

The ripples in Fig. 1 were obtained from a splash rule generated independently of any consideration of ripple dynamics (*7*). [Mean ejecta angle $\bar{\theta} = 64°$ (40° to 130°); mean ejection velocity $\bar{V} = 0.35$ m s^{-1} (0.30 to 1.5 m s^{-1}); mean number of ejecta per impact $\bar{n} = 4.4$ grains.] The splash rule was not adjusted or tuned in any way. Ripples formed, merged, grew (at an ever decreasing rate until further growth became difficult to detect), developed a regular wavelength, exhibited impact shadow zones, and moved downwind much like natural wind ripples.

There are some differences, however, between simulated and natural ripples. The ripples in Fig. 1 are more symmetrical than natural ripples in fine sand, which have less steep stoss slopes, and the simulated ripples shown are several times larger in amplitude (2.3 cm) than most natural eolian sand ripples (*11*). Sensitivity studies in which the mean number of ejected grains per impact was varied from 1.2 to 5.4 produced greater ripple asymmetry but little change in steepness; when the final resting location of an ejected grain was made to depend on slope to reflect a tendency for grains impelled uphill to come to rest before grains impelled downhill, then ripples with lower steepness could be formed. But in all cases the general nature of ripple motion, including merger, growth, repulsion, and regularity, was insensitive to the precise rules used.

In the simulations shown in Fig. 1, impacting grains were deposited by adding them to the distribution of ejected particles. The ripples climbed (*1, 10*) and preserved behind and below them truncated sets of lee-face laminae, as illustrated by the bands of colored grains. In a natural deposit this banding would be visible when some slight variation in sediment supply or sorting led to a distinguishable surface layer that was subsequently buried (*12*). The angle of climb is the arc tangent of the ratio of the vertical motion (due to deposition) to the forward translation (due to reptation) of the bedform. The results in Fig. 1 illustrate subcritical climbing (*13*), in which parts of lee ripple slopes and troughs are preserved. A set of strata associated with each ripple is preserved in the wake of the passage of that ripple and represents all the direct evidence a modern observer has about that ripple's mechanical history.

In Fig. 1, the compressed stratification near the bottom of the deposit reflects the growth and merger of ripples from an initially flat surface; this could represent a new deposition episode under moderate winds on a surface previously planed off by high-velocity storm winds. The direction of travel of the ripple is clear from the slope of the preserved laminae. The vertical thickness of the set of laminations associated with the passage of a single ripple is an increasing function of deposition rate and a decreasing function of forward ripple speed, which depends on the details of the splash function. Mergers of ripples (Fig. 1D) can be identified by irregular trains of laminae, which then serve as an indication of a maturing but not yet mature ripple field. To the extent that the splash function is accurate, paleomechanical impact conditions (speed, angle, and so forth) and therefore information on wind currents and sediment supply can be inferred through trial and error comparison of simulated to natural stratigraphic patterns.

In general, natural impact conditions often will not have remained constant in time. In our simulation, we investigated the effects of a few-minutes-long cessation in deposition during a period of continuing steady wind, as might occur during a fluctuation in the distribution of near-surface wind stress. We modeled this effect by equating the sum of the saltation and reptation fluxes into and out of the model space, so that there was no net gain or loss of bed material. During the depositional hiatus (Fig. 2A) the wind continued to drive ripples forward. Strata climbing from below were planed off; stained surfaces were soon eroded, and the stained grains were reprocessed back into the still translating but no longer climbing ripples. When deposition resumed, climbing translatent strata once again became established, but their history could not be traced backward through the erosion surface. As another example, Fig. 2B shows the beginnings of a cyclic cross-bedding pattern (*14*) resulting from a wind that blew initially from left to right and then reversed directions.

With decreasing ripple speed or increasing rate of deposition, the previously subcritically climbing ripples become critically and then supercritically climbing ripples (*10, 13*). In the latter case stoss surface features are also preserved (Fig. 3). Supercritically climbing laminae are much less common than subcritical laminae in eolian sandstones (*14*). In our simulations, supercritically climbing ripples could not be produced with the use of a splash function for a uniformly sized sand bed. Supercritical deposits could be produced, however, if the mean number of ejected grains per impact was lowered to $\bar{n} = 2.4$. A decrease in $\bar{n}$ from that characteristic of a unimodal sand size distribution might be expected in moderately sorted sands in nature where the finer grains that preferentially populate the saltation cloud are less able to move

coarser bed grains. Supercritical climbing is still difficult to produce without deposition rates of nearly 100% of impacting grains. Further experiment and impact simulation are needed to determine splash dynamics on beds of mixed grain size.

The generic classes of eolian deposits that we have simulated are identifiable in the geologic record. Analytical methods of studying and interpreting such stratigraphy have been discussed by Rubin and Hunter (*15*) and applied mainly to large two-dimensional bedforms. Rubin (*16*) has also described a geometrical model for studying the migration and resulting stratigraphy of three-dimensional bedforms using superpositions of trigonometric functions. The value of the simulations is their basis in the physics of particle behavior after impact. Prevailing wind and sediment conditions at the time of ripple formation and the corresponding bedding structures that are preserved are directly connected through the splash and deposition physics.

REFERENCES AND NOTES

1. J. R. L. Allen, *Sedimentary Structures: Their Character and Physical Basis*, vol. 30A of *Developments in Sedimentology* (Elsevier, Amsterdam, 1982), vol. 1.
2. G. V. Middleton and J. B. Southard, *Mechanics of Sediment Transport* (Short Course No. 3, Society of Economic Paleontologists and Mineralogists, Tulsa, OK, 1984).
3. R. A. Bagnold, *The Physics of Blown Sand and Desert Dunes* (Methuen, London, 1941); R. P. Sharp, *J. Geol.* **71**, 617 (1963); J. F. Kennedy, *J. Geophys. Res.* **69**, 1517 (1964); G. Kocurek, *Sedimentology* **28**, 753 (1981); R. S. Anderson, *ibid.* **34**, 943 (1987); S. G. Fryberger and C. J. Schenk, *Sediment. Geol.* **55**, 1 (1988).
4. J. E. Ungar and P. K. Haff, *Sedimentology* **34**, 289 (1987).
5. B. B. Willetts and M. A. Rice, in *Proceedings of the International Workshop on Physics of Blown Sand*, O. E. Barndorff-Nielson *et al.*, Eds. (Department of Theoretical Statistics, University of Aarhus, Aarhus, Denmark, 1985), mem. 8, vol. 1, p. 83; S. Mitha *et al.*, *Acta Mech.* **63**, 267 (1986); B. T. Werner, thesis, California Institute of Technology, Pasadena (1987).
6. B. T. Werner, *J. Geol.* **98**, 1 (1990).
7. R. S. Anderson and P. K. Haff, *Acta Mech.* (Suppl.) **1**, 21 (1991).
8. ———, *Science* **241**, 820 (1988).
9. P. K. Haff, unpublished data; R. S. Anderson, *Earth-Sci. Rev.* **29**, 77 (1990).
10. R. E. Hunter, *Sedimentology* **24**, 361 (1977).
11. It might be argued that flattening of ripple crests by direct fluid forces remains a possibility. Although not strictly ruled out for an undulating surface, for flat surfaces direct entrainment of grains by the wind is thought to be a small effect compared to impact-induced mobilization (*8*). The sharpness of the ripple crests in Fig. 1 is due to the use of a single impact angle in the simulations.
12. Hunter (*10*) recorded such surfaces by periodically sprinkling a small amount of dark magnetite grains on them.
13. In subcritical climbing the ratio of the rate of vertical motion (due to deposition) to the rate of forward motion is less than the upwind slope of the ripple, so that upwind surfaces are eroded. In supercritical climbing this ratio is greater than the upwind slope, so that upwind surfaces can be preserved in the accumulating column of sediment.
14. R. E. Hunter and D. M. Rubin, in *Eolian Sediments and Processes*, vol. 38 of *Developments in Sedimentology*, M. E. Brookfield and T. S. Ahlbrandt, Eds. (Elsevier, Amsterdam, 1983), pp. 429–454.
15. D. M. Rubin and R. E. Hunter, *Sedimentology* **29**, 121 (1982).
16. D. M. Rubin, *Cross-Bedding, Bedforms, and Paleocurrents* (Society of Economic Paleontologists and Mineralogists, Tulsa, OK, 1987).

17. This work was supported in part by the National Science Foundation [EAR-89-15983] and represents a portion of the work performed by S.B.F. in fulfillment of the requirements for the master's of science degree at Duke University.

17 September 1991; accepted 24 December 1991

Effect of Sodium Salicylate on the Human Heat Shock Response

DONALD A. JURIVICH, LEA SISTONEN, ROGER A. KROES, RICHARD I. MORIMOTO*

Sodium salicylate, an anti-inflammatory agent, was examined for its effects on the heat shock response in cultured human cells. Salicylate activation of DNA binding by the heat shock transcription factor (HSF) was comparable to activation attained during heat shock. However, sodium salicylate did not induce heat shock gene transcription even though the HSF was bound in vivo to the heat shock elements upstream of the heat shock protein 70 (Hsp 70) gene. These results reveal that activation of the heat shock transcriptional response is a multistep process. Modulation of extracellular pH augments sensitivity to salicylate-induced activation of HSF.

THE ANTI-INFLAMMATORY AGENT SODIUM salicylate (*1*) induces heat shock–responsive chromosomal puffs in *Drosophila* salivary glands and stimulates HSF DNA binding activity in cultured *Drosophila* cells (*2, 3*). Inflammation causes a rise in temperature and is accompanied by tissue injury; at the cellular level during inflammation, heat shock and other forms of physiological stress induce the transcription of heat shock genes (*4*). Chondrocytes isolated from inflamed tissues of arthritic patients exhibit unusually high levels of heat shock proteins (*5*). Furthermore, mediators of inflammatory responses, such as the tumor necrosis factor and complement, map adjacent to the Hsp 70 gene on human chromosome 6 (*6*). Therefore, we examined whether salicylate treatment alters the expression of heat shock–inducible genes in human cells.

HeLa cells were exposed to sodium salicylate and short-term–labeled with [^{35}S]methionine, and cellular proteins were analyzed by SDS–polyacrylamide gel electrophoresis. We did not detect additional synthesis of any heat shock proteins over a range of sodium salicylate concentrations (2 to 30 mM) and exposure times (0 to 6 hours). After treatment of cells with 20 mM salicylate, electrophoretic mobility-shift assays were performed with HeLa cell extracts and a heat shock element (HSE) from a human heat shock protein gene. Salicylate activated HSF DNA binding comparable to that obtained with a 42°C heat shock (Fig. 1A). Competition with oligonucleotides showed that salicylate-activated HSF exhibited the same DNA sequence specificity as heat-activated HSF.

We next examined the effect of salicylate on in vivo transcription rates using nuclear run-on analysis. Despite the large amount of HSF DNA binding activity that was induced by salicylate, we did not observe an increase in the transcription rates of either Hsp 70 or Hsp 90 genes (Fig. 1B). Because of this result, we examined whether salicylate-activated HSF DNA binding activity was nuclear-localized and bound in vivo to the HSEs of the Hsp 70 gene. We compared the in vivo occupancy of the HSEs by genomic footprint analysis of the endogenous Hsp 70 gene promoter in salicylate-treated and heat-shocked cells (*5*). The patterns of dimethyl sulfate (DMS) sensitivity for the naked (deproteinated) DNA and control-cell DNA were indistinguishable (Fig. 2A, lanes 1, 2, 6, and 7). The footprint of heat-shocked cells (lanes 3 and 8) indicated HSF binding to five adjacent HSEs corresponding to sites 1, 3, and 5 on the coding strand as well as sites 2 and 4 on the noncoding strand (*7*). The genomic footprint of the cells treated with 20 mM salicylate (lanes 4 and 9) revealed that the salicylate-activated HSF bound in vivo to all five HSE sites. The combination of salicylate and heat shock (lanes 5 and 10) also strongly protected guanine residues known to

D. A. Jurivich, Departments of Medicine and Biochemistry, Molecular Biology, and Cell Biology, Northwestern University, Evanston, IL 60208.
L. Sistonen, R. A. Kroes, R. I. Morimoto, Department of Biochemistry, Molecular Biology, and Cell Biology, Northwestern University, Evanston, IL 60208.

*To whom correspondence should be addressed.